

# 應用於近場紀錄之表面電漿波增強式 C 型奈米波導

研究生: 陳予潔

指導教授: 謝漢萍 教授

國立交通大學光電工程研究所

## 摘要

高密度儲存系統之瓶頸，在於難以取得奈米光點與光輸出量之兼顧。本論文提出一種創新次波長微孔設計，引進奈米波導與表面電漿子的雙重耦合效應，大幅增加穿透場的能量同時仍保持光點大小在奈米之等級。此外，此微孔設計將被應用於光纖之上。由於光纖的輕巧及可撓性，將有利於和既有之磁讀取頭整合成為一個複合式的近場光纖讀取頭。

根據數值分析與最佳化的結果，若與傳統的次波長微孔做比較，光輸出量將可提升  $10^5$ 。實驗的結果，此一微孔設計在近場區域可獲得一個訊噪比為 40 dB 的光學信號，而傳統微孔則因輸出量太低而無法測得；另外，遠場的穿透率也可提升 33 倍。這兩項的實驗結果都可證實在此一微孔設計的近場區域有極強的能量提升，達到一個高密度儲存系統的需求。

# Surface Plasmon Enhanced C-shaped Nano-waveguide for Near-field Recording

**Student: Yu-Chieh Chen**

**Advisor: Prof. Han-Ping D. Shieh**

**Department of Photonics and Institute of Electro-optical Engineering**

## Abstract

The difficulty that a high density storage system encounters lies in giving consideration on both a nano-sized optical spot and an adequate throughput. This thesis proposed an innovative aperture design which possesses the annex of a nano-waveguide and surface plasmon polaritons to substantially increase the throughput at a nano-sized optical spot concomitantly. Besides, this aperture design was fabricated on the end face of a fiber, of which the compactness and flexibility facilitate to be integrated with a magnetic pickup as a near-field hybrid one.

By the analyses and optimization, an enhancement with five orders of magnitude in power throughput was derived; moreover, the implemented experimental results, a near-field transmitted intensity with a signal-noise ratio of 40 dB and a far-field transmission enhancement of 33, evidently demonstrated the strong transmitted field enhancement in the near-field region and fulfilled the requirement of a high-density storage system.

## Acknowledgement

In my two-year graduate life, I am especially grateful to Professor Han-Ping D. Shieh, who gave me many valuable advices and abundant resources. He never told me what the manner to my research should be, but his attitude towards works is just exemplariness to me. Besides, I also appreciate Professor Chung-Hao P. Tien, who gave me many useful feedbacks and suggestions to reap no little benefits.

Besides, my classmates, Moca Chen, Jun-Jay Wang, Chiao-Hen Huang, Hao-Wei Chiu, Zhe-Hung Lin, and Wan-Ling Tsai, have accompanied me during these days and brought me many joys. Those younger classmates, Yen-Hsing Lu, Che-Jen Lin, Wei-Liang Kao, Ming-Jing Chieh and Chieh-Hsiang Hung, and those senior classmates, Ko-Wei Dodu Chieh, Yi-Pei Bounds Huang, Po-Ru Paul Yang, Chiao-Shun Patric Chuang, An-Chi Angel Wei, Chi-Huan Lionel Lee and Chun-Ho Chen, all helped me a lot in my life. Certainly, the beautiful, kind and sweet secretaries, particularly Miss Vivian Ni, also aided me a lot in administration affairs. Moreover, the French international students, Lucie, Lilian and Thibault made my last half semester colorful. Anyhow, I would like to show my gratitude to these abovementioned people.

I also heartfully appreciate my senior classmate and my boyfriend, Jen-Yu Ray Fang for his wholehearted supports in academic study and in affection, keeping with me regardless of merriness or sorrow. His encouragement and love greatly motivates the birth of this thesis.

Finally, I have to extremely owe my most lofty esteem to my parents, my grandmother and my lovely younger brother, who always support me silently and love me endlessly. What I may accomplish today is inevitably cultivated by what they devoted to me.

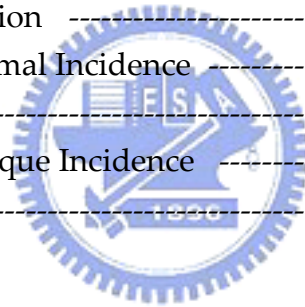
Without these people, this thesis would never have seen the light of day.

Yu-Chieh Ricca Chen in June, 2005

# Table of Contents

Abstract (Chinese) -----	i
Abstract (English) -----	ii
Acknowledgement -----	iii
Table of Contents -----	iv
Figure Captions -----	vii
List of Tables -----	xii
<b>Chapter 1 Introduction -----</b>	<b>1</b>
1.1 Motivation-----	1
1.2 Objectives -----	4
1.3 Organization -----	5
<b>Chapter 2 Theory and Literature Survey -----</b>	<b>6</b>
2.1 Bethe's Theory -----	6
2.1.1 Mathematical Formulation and Physical Assumption -----	6
2.1.2 Determination of Surface Magnetic Charge/Current Density -----	9
2.1.3 Boundary Condition for Normal Component of Electric Field-----	11
2.1.4 Evaluation of Electric/Magnetic and Total Radiation -----	12
2.1.5 Power Throughput and Discussion -----	12
2.2 Finite-Difference Time-Domain Method -----	14
2.3 Surface Plasmon Polariton -----	16
2.4 Special Shaped Aperture -----	21
2.4.1 Scatter-formed Aperture -----	21
2.4.2 Triangular Aperture -----	22
2.4.3 C-shaped Aperture -----	23
2.4.4 I-shaped Aperture -----	24
2.5 Surface Corrugation -----	26
2.6 Summary -----	29
<b>Chapter 3 Simulation – Optimization of C-aperture -----</b>	<b>30</b>
3.1 Simulation Description -----	30

3.1.1 Optical Model .....	30
3.1.2 Parameters .....	31
3.1.3 Evaluation Factors .....	31
3.2 Results (1) – Freestanding case .....	33
3.2.1 Square Aperture .....	33
3.2.2 C-aperture with Fixed Aperture Parts .....	34
3.2.3 C-aperture with Fixed Ridge Parts .....	36
3.2.4 Correspondence Relation .....	38
3.2.5 Comparison (1) – Normal Incidence .....	43
3.2.6 Oblique Incidence .....	46
3.2.7 Comparison (2) – Oblique Incidence .....	48
3.3 Results (2) – Integrated case .....	49
3.3.1 Square Aperture .....	49
3.3.2 Index Matching .....	50
3.3.2 C-aperture with Fixed Aperture Parts .....	51
3.3.3 C-aperture with Fixed Ridge Parts .....	54
3.3.4 Correspondence Relation .....	56
3.3.5 Comparison (1) – Normal Incidence .....	59
3.3.6 Oblique Incidence .....	61
3.3.7 Comparison (2) – Oblique Incidence .....	63
3.4 Summary - .....	64



**Chapter 4 Simulation – C-aperture with Surface Corrugation ----- 66**

4.1 Simulation Description .....	66
4.1.1 Optical Model .....	66
4.1.2 Parameters .....	66
4.1.3 Evaluation Factors .....	66
4.2 Results (1) – Incident-side Groove .....	68
4.2.1 Rectangular Aperture .....	68
4.2.2 C-shaped Aperture .....	69
4.3 Results (2) – Exit-side Groove .....	74
4.4 Summary .....	78

**Chapter 5 Experiment ----- 79**

5.1 Instruments .....	79
5.1.1 Focused Ion Beam (FIB) .....	79

5.1.2 Near-field Scanning Optical Microscopy (NSOM) -----	80
5.1.3 Fiber-based Transmission Measurement System (FTMS) -----	82
5.2 Results -----	83
5.2.1 Sample Preparation -----	83
5.2.2 Near-field Distribution - -----	84
5.2.3 Far-field Transmission -----	85
5.3 Summary -----	87
<b>Chapter 6 Conclusion and Future Work -----</b>	<b>88</b>
6.1 Conclusion -----	88
6.2 Future Work -----	90
<b>Reference -----</b>	<b>91</b>



# Figure Captions

## Chapter 1 Introduction

### 1.1 Motivation

Fig. 1.1-1 Layout of an SIL .....	2
Fig. 1.1-2 An SIL-based flying pickup .....	2
Fig. 1.1-3 Betzig's experimental result .....	3

### 1.2 Objectives

Fig. 1.2-1 Primary model of fiber-based light delivery module .....	4
Fig. 1.2-2 Improved model of fiber-based light delivery module .....	4

## Chapter 2 Theory and Literature Survey

### 2.1 Bethe's Theory

Fig. 2.1-1 Model of Bethe's theory .....	7
Fig. 2.1-2 Diagram of source point and field point .....	9

### 2.2 Finite-Difference Time-Domain Method

Fig. 2.2-1 Unit cell of FDTD mesh .....	14
---	----

### 2.3 Surface Plasmon Polaritons

Fig. 2.3-1 SPPs on metal film interfaces with lossless dielectric materials .....	17
Fig. 2.3-2 Geometry of a periodically structured metal film .....	18
Fig. 2.3-3 Schematics of tunneling processes through a metal film .....	20
(a) no resonant SPP mode	
(b) SPP modes excited on one of the film interfaces	
(c) SPP modes excited on both interfaces in symmetric surroundings	
(d) SPP modes excited on both interfaces in asymmetric surroundings	

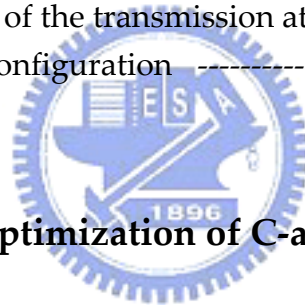
### 2.4 Special Shaped Aperture

Fig. 2.4-1 Model of planar aperture-mounted head with a minute scatterer .....	21
Fig. 2.4-2 Energy intensity profiles of the scatterer-formed aperture .....	22
(a) along X-direction	
(b) along Y-direction	
Fig. 2.4-3 Model of a near-field optical head with a triangular aperture .....	22

Fig. 2.4-4 Energy distribution of the triangular aperture .....	23
Fig. 2.4-5 Optical model of the C-shaped aperture .....	23
Fig. 2.4-6 Electric field intensity distribution at 48 nm from .....	24
(a) square aperture	
(b) C-shaped aperture	
Fig. 2.4-7 Parameters of an I-shaped aperture .....	24
Fig. 2.4-8 Electric energy distribution of .....	25
(a) square aperture of $0.064\lambda \times 0.064\lambda$	
(b) I-shaped aperture with gap area of $0.064\lambda \times 0.064\lambda$	

## 2.5 Surface Corrugation

Fig. 2.5-1 Single aperture surrounded by surface corrugations .....	26
(a) side view	
(b) top view	
Fig. 2.5-2 Transmission spectra of a single aperture of diameter 440 surrounded by surface corrugation of pitch 750 nm with various corrugation depth ----	27
Fig. 2.5-3 Angular dependence of the transmission at the resonant wavelength of a double-corrugated configuration .....	27



## Chapter 3 Simulation – Optimization of C-aperture

### 3.1 Simulation Description

Fig. 3.1-1 Optical models of .....	31
(a) freestanding case	
(b) integrated case	
Fig. 3.1-2 Parameter of C-aperture .....	31
Fig. 3.1-3 Schematics of .....	32
(a) power throughput	
(b) photons incapable of tunneling	
(c) photons captured by the aperture	

### 3.2 Results (1) – Freestanding Case

Fig. 3.2-1 Power throughput of square apertures with varied sides .....	33
Fig. 3.2-2 Power throughput density of square apertures with varied sides .....	34
Fig. 3.2-3 Power throughput of C-apertures with varied gap parts .....	35
Fig. 3.2-4 Power throughput density of C-apertures with varied gap parts .....	36
Fig. 3.2-5 Power throughput of C-apertures with varied aperture parts .....	37

Fig. 3.2-6 Power throughput density of C-apertures with varied aperture parts	---	38
Fig. 3.2-7 Power throughput of C-aperture with varied aperture parts	-----	39
(a) ridge width of 34 nm		
(b) ridge width of 46 nm		
(c) ridge width of 58 nm		
(d) ridge width of 70 nm		
(e) ridge width of 82 nm		
Fig. 3.2-8 Electric field energy density of	-----	45
(a) 60*60 nm <sup>2</sup> square aperture		
(b) the optimum C-aperture		
Fig. 3.2-9 Schematics of	-----	46
(a) definition of phi and theta		
(b) C-aperture dimensions		
Fig. 3.2-10 Power throughput as a function of incident angle phi	-----	47
Fig. 3.2-11 Power throughput as a function of incident angle theta	-----	48

### 3.3 Results (2) – Integrated Case

Fig. 3.3-1 Power throughput of square apertures with varied sides	-----	49
Fig. 3.3-2 Power throughput density of square apertures with varied sides	-----	50
Fig. 3.3-3 Diagrams of isometric downsizing for index matching	-----	50
Fig. 3.3-4 Power throughput as functions of scale factor and refractive index	-----	51
Fig. 3.3-5 Parameters of downsized C-aperture with varied gap parts	-----	52
Fig. 3.3-6 Power throughput of C-apertures with varied gap parts	-----	52
Fig. 3.3-7 Power throughput density of C-apertures with varied gap parts	-----	53
Fig. 3.3-8 Parameters of downsized C-aperture with varied aperture parts	-----	54
Fig. 3.3-9 Power throughput of C-apertures with varied aperture parts	-----	54
Fig. 3.3-10 Power throughput density of C-apertures with varied aperture parts	--	55
Fig. 3.3-11 Power throughput of C-aperture with varied aperture parts	-----	56
(a) ridge width of 23.1 nm		
(b) ridge width of 31.2 nm		
(c) ridge width of 39.3 nm		
(d) ridge width of 55.6 nm		
Fig. 3.3-12 Electric field energy density of	-----	60
(a) 60*60 nm <sup>2</sup> square aperture		
(b) the optimum C-aperture		
Fig. 3.3-13 Schematics of	-----	61
(a) definition of phi and theta		
(b) C-aperture dimensions		

Fig. 3.3-14 Power throughput as a function of incident angle $\phi$	62
Fig. 3.3-15 Power throughput as a function of incident angle $\theta$	62

## Chapter 4 Simulation – Surface Corrugation

### 4.1 Simulation Description

Fig. 4.1-1 Schematics of	66
(a) C-aperture dimensions	
(b) Parameters of a groove	

### 4.2 Results (1) – Incident-side Groove

Fig. 4.2-1 Configurations of a rectangular aperture with a groove	68
Fig. 4.2-2 Power throughput of various rectangular apertures	69
Fig. 4.2-3 Parameters of an incident-side-corrugated C-aperture	70
Fig. 4.2-4 Power throughput of incident-side-corrugated C-aperture as functions of interval and width	71
Fig. 4.2-5 Power throughput of incident-side-corrugated C-aperture as functions of interval and pitch	72
Fig. 4.2-6 Configurations of	73
(a) square aperture	
(b) optimum C-aperture	
(c) optimum incident-side-corrugated C-aperture	



### 4.3 Results (2) – Exit-side Groove

Fig. 4.3-1 Parameters of an double-side-corrugated C-aperture	74
(a) incident face	
(b) exit face	
Fig. 4.3-2 Power throughput of double-side-corrugated C-aperture as functions of interval and width	75
Fig. 4.3-3 Spot size of double-side-corrugated C-aperture as functions of interval and width	76
Fig. 4.3-4 Power throughput density of double-side-corrugated C-aperture as functions of interval and width	77

### 4.4 Summary

Fig. 4.4-1 Configurations of	78
(a) square aperture	

- (b) optimum C-aperture
- (c) optimum incident-side-corrugated C-aperture
- (d) optimum double-side-corrugated C-aperture

## Chapter 5 Experiment

### 5.1 Instruments

Fig. 5.1-1 Operation principle of FIB system .....	79
Fig. 5.1-2 Dual beam systems (FIB/SEM) in .....	80
(a) PIDC	
(b) CMU	
Fig. 5.1-3 Schematics of shear force regulation mechanism .....	81
Fig. 5.1-4 NSOM in Academia Sinica of .....	81
(a) reflection mode	
(b) transmission mode	
Fig. 5.1-5 Fiber-based Transmission measurement system .....	82
(a) schematics	
(b) photo	



### 5.2 Results

Fig. 5.2-1 SEM photons of .....	83
(a) alignment key	
(b) circular aperture	
Fig. 5.2-2 SEM photons of .....	84
(a) alignment key	
(b) C-aperture	
Fig. 5.2-3 SEM photons of incident-side-corrugated C-aperture .....	84
Fig. 5.2-4 Optical signal detected by NSOM of .....	85
(a) background noise	
(b) C-aperture	

## Chapter 6 Conclusion and Future Work

### 6.2 Future Works

Fig. 6.2-1 Fiber-based light delivery module in realization of hybrid recording ----	90
--	----

# List of Tables

## Chapter 3 Simulation – Optimization of C-aperture

### 3.2 Results (1) – Freestanding Case

Table 3.2-1 Spot size of square apertures with varied sides -----	34
Table 3.2-2 Spot size of C-apertures with varied gap parts -----	35
(a) X-direction	
(b) Y-direction	
Table 3.2-3 Spot size of C-apertures with varied aperture parts -----	38
(a) X-direction	
(b) Y-direction	
Table 3.2-4 $AR_{\text{peak}}$ of the C-aperture with different aperture length and ridge width -----	42
Table 3.2-5 Gap corresponding to each $AR_{\text{peak}}$ in Table 3.2-4 -----	42
Table 3.2-6 Quantity of correspondence relation -----	43
Table 3.2-7 Comparison of a $60 \times 60 \text{ nm}^2$ square aperture and the optimum C-aperture -----	44
Table 3.2-8 Spot size at different incident angle phi -----	47
Table 3.2-9 Spot size at different incident angle theta -----	48
Table 3.2-10 Comparison of a $60 \times 60 \text{ nm}^2$ square aperture and the optimum C-aperture at incident angle $(\Phi, \theta)$ of $(-27^\circ, 0^\circ)$ -----	48

### 3.3 Results (2) – Integrated Case

Table 3.3-1 Spot size of square apertures with varied sides -----	49
Table 3.3-2 Spot size of C-apertures with varied gap parts -----	53
(c) X-direction	
(d) Y-direction	
Table 3.3-3 Spot size of C-apertures with varied aperture parts -----	55
(c) X-direction	
(d) Y-direction	
Table 3.3-4 Quantity of correspondence relation -----	59
Table 3.3-5 Comparison of a $60 \times 60 \text{ nm}^2$ square aperture and the optimum C-aperture -----	59
Table 3.3-6 Spot size at different incident angle phi -----	62
Table 3.3-7 Spot size at different incident angle theta -----	62
Table 3.3-8 Comparison of a $60 \times 60 \text{ nm}^2$ square aperture and the optimum C-aperture at incident angle $(\Phi, \theta)$ of $(-39^\circ, 0^\circ)$ -----	63

## Chapter 4 Simulation – Surface Corrugation

### 4.2 Results (1) – Incident-side Groove

Table 4.2-1 Coupling efficiency of various rectangular apertures ----- 69

Table 4.2-2 Comparison of square aperture, optimum C-aperture and optimum incident-side-corrugated C-aperture ----- 73

### 4.3 Results (2) – Exit-side Groove

Table 4.3-1 Spot size of double-side-corrugated C-aperture ----- 76

(a) X-direction

(b) Y-direction

### 4.4 Summary

Table 4.4-1 Comparison of the square aperture, optimum C-aperture, optimum incident-side-corrugated C-aperture and double-side-corrugated C-aperture ----- 78

## Chapter 5 Experiment

### 5.2 Results

Table 5.2-1 Measured transmission and calculated enhancements ----- 86

